A test of the Suyama-Yamaguchi inequality from weak lensing

Article (Published Version)

Monthly Notices
of the
ROYAL ASTRONOMICAL SOCIETY

MNRAS **442,** 1068–1078 (2014) doi:10.1093/mnras/stu900

A test of the Suyama–Yamaguchi inequality from weak lensing

Alessandra Grassi,[1] Lavinia Heisenberg,[2,3] Christian T. Byrnes[4] and Björn Malte Schäfer[1]★

[1]*Astronomisches Recheninstitut, Zentrum für Astronomie, Universität Heidelberg, Philosophenweg 12, D-69120 Heidelberg, Germany*
[2]*Département de Physique Théorique and Center for Astroparticle Physics, Université de Genève, 24 Quai E. Ansermet, CH-1211 Genève, Switzerland*
[3]*Department of Physics, Case Western Reserve University, 10900 Euclid Ave, Cleveland, OH 44106, US*
[4]*Department of Physics and Astronomy, University of Sussex, Brighton BN1 9RH, UK*

Accepted 2014 May 5. Received 2014 April 25; in original form 2013 July 16

ABSTRACT

We investigate the weak lensing signature of primordial non-Gaussianities of the local type by constraining the magnitude of the weak convergence bi- and trispectra expected for the *Euclid* weak lensing survey. Starting from expressions for the weak convergence spectra, bispectra and trispectra, whose relative magnitudes we investigate as a function of scale, we compute their respective signal-to-noise ratios by relating the polyspectra's amplitude to their Gaussian covariance using a Monte Carlo technique for carrying out the configuration space integrations. In computing the Fisher matrix on the non-Gaussianity parameters $f_{\rm NL}$, $g_{\rm NL}$ and $\tau_{\rm NL}$ with a very similar technique, we can derive pieces of Bayesian evidence for a violation of the Suyama–Yamaguchi (SY) relation $\tau_{\rm NL} \geq (6f_{\rm NL}/5)^2$ as a function of the true $f_{\rm NL}$- and $\tau_{\rm NL}$-values and show that the relation can be probed down to levels of $f_{\rm NL} \simeq 10^2$ and $\tau_{\rm NL} \simeq 10^5$. In a related study, we derive analytical expressions for the probability density that the SY relation is exactly fulfilled, as required by models in which any one field generates the perturbations. We conclude with an outlook on the levels of non-Gaussianity that can be probed with tomographic lensing surveys.

Key words: gravitational lensing: weak – methods: analytical – inflation.

1 INTRODUCTION

Advances in observational cosmology has made it possible to probe models of the early Universe and the mechanisms that can generate small seed perturbations in the density field from which the cosmic large-scale structure grew by gravitational instability. One of the most prominent of these models is inflation, in which the Universe underwent an extremely rapid exponential expansion and where small fluctuations in the inflationary field gave rise to fluctuations in the gravitational potential and which then imprinted these fluctuations on to all cosmic fluids (for reviews, see Bartolo et al. 2004; Seery, Lidsey & Sloth 2007; Komatsu et al. 2009; Desjacques & Seljak 2010a,b; Komatsu 2010; Verde 2010; Jeong, Schmidt & Sefusatti 2011; Lesgourgues 2013; Martin, Ringeval & Vennin 2013; Wang 2013). Observationally, inflationary models can be distinguished by the spectral index $n_{\rm s}$ along with a possible scale dependence, the scalar-to-tensor ratio r and, perhaps most importantly, the non-Gaussian signatures, quantified by n-point correlation functions or by polyspectra of order n in Fourier space. They are of particular interest as there is a relation between the statistical properties of the fields and its dynamics. Additionally, the configuration space dependence of the polyspectra yields valuable information on the type of inflationary model (Byun & Bean 2013).

The (possibly non-Gaussian) density fluctuations are subsequently imprinted in the cosmic microwave background (CMB) as temperature anisotropies (Fergusson & Shellard 2007, 2009; Vielva & Sanz 2009; Fergusson, Liguori & Shellard 2010a; Pettinari et al. 2013), in the matter distribution which can be probed by e.g. gravitational lensing and in the number density of galaxies. Hereby, it is advantageous that the observable is linear in the field whose statistical property we investigate. In case of linear dependence, the n-point functions of the observable field can be mapped directly on to the corresponding n-point function of the primordial density perturbation, which reflects the microphysics of the early Universe.

The first important measurement quantifying non-Gaussianity is the parameter $f_{\rm NL}$ which describes the skewness of inflationary fluctuations and determines the amplitude of the bispectrum. Not only the bispectrum but also the trispectrum can successfully be constrained by future precisions measurements, where the parameters $g_{\rm NL}$ and $\tau_{\rm NL}$ determine the trispectrum amplitude. The complementary analysis of both the bi- and the trispectra in the future experiments will make us able to extract more information about the mechanism of generating the primordial curvature perturbations and constrain the model of the early Universe. Therefore, it is an indispensable task for cosmology to obtain the configuration space

★E-mail: bjoern.malte.schaefer@uni-heidelberg.de

dependence for the higher polyspectra and to make clear predictions for the non-Gaussianity parameters. The non-Gaussianities are commonly expressed as perturbations of modes of the potential $\propto k^{n_s/2-2}$ but can in principle have scale dependences (Chen 2005; Lo Verde et al. 2008; Sefusatti et al. 2009; Byrnes, Enqvist & Takahashi 2010a; Byrnes et al. 2010b; Becker, Huterer & Kadota 2011; Riotto & Sloth 2011).

The first cosmological data release of the *Planck* satellite has resulted in the tightest ever constraints on $f_{\rm NL}$ and $\tau_{\rm NL}$ (Planck Collaboration: Ade et al. 2013a). For the local bispectrum, $f_{\rm NL} = 2.7 \pm 5.8$, with the 1σ confidence level quoted, while the 95 per cent upper bound on the trispectrum parameter is $\tau_{\rm NL} \leq 2800$. The $f_{\rm NL}$ is about a factor of 4 improvement over the *Wilkinson Microwave Anisotropy Probe* bound (*WMAP*; Bennett et al. 2013; Giannantonio et al. 2014), while the $\tau_{\rm NL}$ bound is improved by about an order of magnitude (Hikage & Matsubara 2012). No *Planck* bound on $g_{\rm NL}$ has yet been made, the tightest bound is currently $g_{\rm NL} = (-3.3 \pm 2.2) \times 10^5$ from *WMAP*9 data (Sekiguchi & Sugiyama 2013). Previous CMB constraints were made in Hikage et al. (2008), Smidt et al. (2010a) and Fergusson, Regan & Shellard (2010b). The bound on $f_{\rm NL}$ is close to cosmic variance limited for any CMB experiment, for the trispectrum parameters the bounds may still improve by a factor of a few, see e.g. Smidt et al. (2010a), Fergusson et al. (2010a) and Sekiguchi & Sugiyama (2013).

An alternative way of constraining non-Gaussianities are the number density of clusters as a function of their mass, see Fedeli et al. (2011b), LoVerde & Smith (2011) and Enqvist, Hotchkiss & Taanila (2011) who show that constraints of the order of 10^2 on $f_{\rm NL}$ and 10^8 on $g_{\rm NL}$.

In comparison to other probes, weak gravitational lensing provides weaker bounds, but non-Gaussianities have nevertheless important implications for weak lensing. Although the weak lensing bispectrum is by far dominated by structure formation non-Gaussianities (Bernardeau, van Waerbeke & Mellier 2003; Takada & Jain 2003, 2004), whose observational signature has been detected at high significance (via the quasar magnification bias and the aperture mass skewness; Ménard, Bartelmann & Mellier 2003; Semboloni et al. 2011b, respectively), there are a number of studies focusing on primordial non-Gaussianities, for example weak lensing peak counts (Marian et al. 2011), yielding $\sigma_{f_{\rm NL}} \simeq 10$ constraints on non-Gaussianities, or topological measures of the weak lensing map, for instance the skeleton (Fedeli et al. 2011a) or Minkowski functionals (Munshi et al. 2012). Direct estimation of the inflationary weak lensing bispectra is possible (Pace et al. 2011; Schäfer et al. 2012) but suffers from the Gaussianizing effect of the line-of-sight integration (Jeong et al. 2011). Similar to the weak lensing spectrum, bispectra also suffer from contamination by intrinsic alignments (Semboloni et al. 2008) and baryonic physics (Semboloni et al. 2011a).

The description of inflationary non-Gaussianities is done in a perturbative way, and for the relative magnitude of non-Gaussianities of different order, the Suyama–Yamaguchi (SY) relation applies (Suyama & Yamaguchi 2008; Suyama et al. 2010; Lewis 2011; Smith, Loverde & Zaldarriaga 2011b; Assassi, Baumann & Green 2012; Kehagias & Riotto 2012; Sugiyama 2012; Beltrán Almeida, Rodríguez & Valenzuela-Toledo 2013; Rodríguez et al. 2013; Tasinato et al. 2013), which in the most basic form relates the amplitudes of the bi- and of the trispectrum. Recently, it has been proposed that testing for a violation of the SY-inequality would make it possible to distinguish between different classes of inflationary models. In this work, we focus on the relation between the non-Gaussianity parameters $f_{\rm NL}$ and $\tau_{\rm NL}$ for a local model, and investigate how well the future *Euclid* survey can probe the SY-relation. The question we address is how likely would we believe in the SY-inequality with the inferred $f_{\rm NL}$ and $\tau_{\rm NL}$-values. We accomplish this by studying the Bayesian evidence (Trotta 2007, 2008) providing support for the SY-inequality.

Models in which a single field generates the primordial curvature perturbation predict an equality between one term of the trispectrum and the bispectrum, $(\tau_{\rm NL} = (6f_{\rm NL}/5)^2$, provided that the loop corrections are not anomalously large, if they are then $g_{\rm NL}$ should also be observable; Tasinato et al. 2013). Violation of this consistency relation would prove that more than one light field present during inflation had to contribute towards the primordial curvature perturbation. However, a verification of the equality would not imply single field inflation, rather that only one of the fields generated perturbations. In fact, any detection of non-Gaussianity of the local form will prove that more than one field was present during inflation, because single field inflation predicts negligible levels of local non-Gaussianity. A detection of $\tau_{\rm NL} > (6f_{\rm NL}/5)^2$ would prove that not only that inflation was of the multifield variety, but also that multiple fields contributed towards the primordial perturbations, which are the seeds which gave rise to all the structure in the Universe today. Weaker forms of the SY-relation, $\tau_{\rm NL} > (6/5f_{\rm NL})^2/2$, has been proposed by Sugiyama, Komatsu & Futamase (2011) for multifield-inflationary models, although these may have been refuted by Smith, Loverde & Zaldarriaga (2011b).

A violation of the SY-inequality would come as a big surprise, since the inequality has been proved to hold for all models of inflation. Even more strongly, in the limit of an infinite volume survey it holds true simply by the definitions of $\tau_{\rm NL}$ and $f_{\rm NL}$, regardless of the theory relating to the primordial perturbations. However, since realistic surveys will always have a finite volume, a breaking of the inequality could occur. It remains unclear how one should interpret a breaking of the inequality, and whether any concrete scenarios can be constructed in which this would occur. A violation may be related to a breaking of statistical homogeneity (Smith et al. 2011b).

After a brief summary of cosmology and structure formation in Section 2, we introduce primordial non-Gaussianities in Section 3 along with the SY-inequality relating the relative non-Gaussianity strengths in the polyspectra of different order. The mapping of non-Gaussianities by weak gravitational lensing is summarized in Section 4. Then, we investigate the attainable signal-to-noise ratios (Section 5), address degeneracies in the measurement of $g_{\rm NL}$ and $\tau_{\rm NL}$ in Section 6, carry out statistical tests of the SY-inequality (Section 7), investigate analytical distributions of ratios of non-Gaussianity parameters (Section 8) and quantify the Bayesian evidence for a violation of the SY-inequality from a lensing measurement (Section 9). We summarize our main results in Section 10.

The reference cosmological model used is a spatially flat w cold dark matter (CDM) cosmology with adiabatic initial perturbations for the CDM. The specific parameter choices are $\Omega_{\rm m} = 0.25$, $n_{\rm s} = 1$, $\sigma_8 = 0.8$, $\Omega_{\rm b} = 0.04$. The Hubble parameter is set to $h = 0.7$ and the Hubble distance is given by $c/H_0 = 2996.9\,{\rm Mpc}\,h^{-1}$. The dark energy equation of state is assumed to be constant with a value of $w = -0.9$. We prefer to work with these values that differ slightly from the recent *Planck* results (Planck Collaboration: Ade et al. 2013b) because lensing prefers lower $\Omega_{\rm m}$-values and larger h-values (Heymans et al. 2013). Scale invariance for $n_{\rm s}$ was chosen for simplicity and should not strongly affect the conclusions as the range of angular scales probed is small and close to the normalization scale.

The fluctuations are taken to be Gaussian perturbed with weak non-Gaussianities of the local type, and for the weak lensing survey

we consider the case of *Euclid*, with a sky coverage of $f_{\rm sky} = 1/2$, a median redshift of 0.9, a yield of $\bar{n} = 40$ galaxies arcmin^{-2} and a ellipticity shape noise of $\sigma_\epsilon = 0.3$ (Amara & Réfrégier 2007; Refregier 2009).

2 COSMOLOGY AND STRUCTURE FORMATION

In spatially flat dark energy cosmologies with the matter density parameter $\Omega_{\rm m}$, the Hubble function $H(a) = {\rm d}\ln a/{\rm d}t$ is given by

$$\frac{H^2(a)}{H_0^2} = \frac{\Omega_{\rm m}}{a^3} + \frac{1-\Omega_{\rm m}}{a^{3(1+w)}}, \tag{1}$$

for a constant dark energy equation-of-state parameter w. The comoving distance χ and scale factor a are related by

$$\chi = c\int_a^1 \frac{{\rm d}a}{a^2 H(a)}, \tag{2}$$

given in units of the Hubble distance $\chi_{\rm H} = c/H_0$. For the linear matter power spectrum $P(k)$ which describes the Gaussian fluctuation properties of the linearly evolving density field δ,

$$\langle\delta(\boldsymbol{k})\delta(\boldsymbol{k}')\rangle = (2\pi)^3\delta_D(\boldsymbol{k}+\boldsymbol{k}')P(k) \tag{3}$$

the ansatz $P(k) \propto k^{n_{\rm s}}T^2(k)$ is chosen with the transfer function $T(k)$, which is well approximated by the fitting formula

$$T(q) = \frac{\ln(1+2.34q)}{2.34q}\times\left[1+3.89q+(16.1q)^2 + (5.46q)^3+(6.71q)^4\right]^{-1/4}, \tag{4}$$

for low-matter density cosmologies (Bardeen et al. 1986). The wave vector $k = q\Gamma$ enters rescaled by the shape parameter Γ (Sugiyama 1995),

$$\Gamma = \Omega_{\rm m}h\exp\left[-\Omega_{\rm b}\left(1+\frac{\sqrt{2h}}{\Omega_{\rm m}}\right)\right]. \tag{5}$$

The fluctuation amplitude is normalized to the variance σ_8^2,

$$\sigma_R^2 = \int\frac{k^2{\rm d}k}{2\pi^2}\,W_R^2(k)\,P(k), \tag{6}$$

with a Fourier-transformed spherical top-hat $W_R(k) = 3j_1(kR)/(kR)$ as the filter function operating at $R = 8\,{\rm Mpc}\,h^{-1}$. $j_\ell(x)$ denotes the spherical Bessel function of the first kind of the order of ℓ (Abramowitz & Stegun 1972). The linear growth of the density field, $\delta(\boldsymbol{x}, a) = D_+(a)\delta(\boldsymbol{x}, a=1)$, is described by the growth function $D_+(a)$, which is the solution to the growth equation (Turner & White 1997; Wang & Steinhardt 1998; Linder & Jenkins 2003),

$$\frac{{\rm d}^2}{{\rm d}a^2}D_+(a) + \frac{1}{a}\left(3+\frac{{\rm d}\ln H}{{\rm d}\ln a}\right)\frac{\rm d}{{\rm d}a}D_+(a) = \frac{3}{2a^2}\Omega_{\rm m}(a)D_+(a). \tag{7}$$

From the CDM spectrum of the density perturbation, the spectrum of the Newtonian gravitational potential can be obtained

$$P_\Phi(k) = \left(\frac{3\Omega_{\rm m}}{2\chi_{\rm H}^2}\right)^2 k^{n_{\rm s}-4}\,T(k)^2 \tag{8}$$

by application of the Poisson equation which reads $\Delta\Phi = 3\Omega_{\rm m}/(2\chi_{\rm H}^2)\delta$ in comoving coordinates at the current epoch, $a = 1$.

3 NON-GAUSSIANITIES

Inflation has been a very successful paradigm for understanding the origin of the perturbations we observe in different observational channels today. It explains in a very sophisticated way how the Universe was smoothed during a quasi-de Sitter expansion while allowing quantum fluctuations to grow and become classical on super-horizon scales. In its simplest implementation, inflation generically predicts almost Gaussian density perturbations close to scale invariance. In the most basic models of inflation, fluctuations originate from a single scalar field in approximate slow roll and deviations from the ideal Gaussian statistics is caused by deviations from the slow-roll conditions. Hence, a detection of non-Gaussianity would be indicative of the shape of the inflaton potential or would imply a more elaborate inflationary model. Although there is consensus that competitive constraints on the non-Gaussianity parameters will emerge from CMB observations and the next generation of large-scale structure experiments, non-Gaussianities beyond the trispectrum will remain difficult if not impossible to measure. For that reason, we focus on the extraction of bi- and trispectra from lensing data and investigate constraints on their relative magnitude.

Local non-Gaussianities are described as quadratic and cubic perturbations of the Gaussian potential $\Phi_{\rm G}(\boldsymbol{x})$ at a fixed point $\boldsymbol{x}$, which yields in the single-source case the resulting field $\Phi(\boldsymbol{x})$ (LoVerde & Smith 2011),

$$\Phi_{\rm G}(\boldsymbol{x}) \to \Phi(\boldsymbol{x}) = \Phi_{\rm G}(\boldsymbol{x}) + f_{\rm NL}\left(\Phi_{\rm G}^2(\boldsymbol{x}) - \langle\Phi_{\rm G}^2\rangle\right) + g_{\rm NL}\left(\Phi_{\rm G}^3(\boldsymbol{x}) - 3\langle\Phi_{\rm G}^2\rangle\Phi_{\rm G}(\boldsymbol{x})\right), \tag{9}$$

with the parameters $f_{\rm NL}$, $g_{\rm NL}$ and $\tau_{\rm NL}$. These perturbations generate in Fourier space a bispectrum $\langle\Phi(\boldsymbol{k}_1)\Phi(\boldsymbol{k}_2)\Phi(\boldsymbol{k}_3)\rangle = (2\pi)^3\delta_D(\boldsymbol{k}_1+\boldsymbol{k}_2+\boldsymbol{k}_3)\,B_\Phi(\boldsymbol{k}_1,\boldsymbol{k}_2,\boldsymbol{k}_3)$,

$$B_\Phi(\boldsymbol{k}_1,\boldsymbol{k}_2,\boldsymbol{k}_3) = \left(\frac{3\Omega_{\rm m}}{2\chi_{\rm H}^2}\right)^3 2f_{\rm NL}\left((k_1k_2)^{n_{\rm s}-4} + 2\ \text{perm.}\right) \times T(k_1)T(k_2)T(k_3) \tag{10}$$

and a trispectrum $\langle\Phi(\boldsymbol{k}_1)\Phi(\boldsymbol{k}_2)\Phi(\boldsymbol{k}_3)\Phi(\boldsymbol{k}_4)\rangle = (2\pi)^3\delta_D(\boldsymbol{k}_1+\boldsymbol{k}_2+\boldsymbol{k}_3+\boldsymbol{k}_4)\,T_\Phi(\boldsymbol{k}_1,\boldsymbol{k}_2,\boldsymbol{k}_3,\boldsymbol{k}_4)$,

$$T_\Phi(\boldsymbol{k}_1,\boldsymbol{k}_2,\boldsymbol{k}_3,\boldsymbol{k}_4) = \left(\frac{3\Omega_{\rm m}}{2\chi_{\rm H}^2}\right)^4\left[6g_{\rm NL}\left((k_1k_2k_3)^{n_{\rm s}-4} + 3\ \text{perm.}\right) + \frac{25}{9}\tau_{\rm NL}\left(k_1^{n_{\rm s}-4}k_3^{n_{\rm s}-4}\,|\boldsymbol{k}_1+\boldsymbol{k}_2|^{n_{\rm s}-4} + 11\ \text{perm.}\right)\right] \times T(k_1)T(k_2)T(k_3)T(k_4). \tag{11}$$

The normalization of each mode $\Phi(\boldsymbol{k})$ is derived from the variance σ_8^2 of the CDM spectrum $P(k)$.

Calculating the four-point function of equation (9), one would find the coefficient $(2f_{\rm NL})^2$ instead of the factor $25\tau_{\rm NL}/9$ in equation (11) (see Byrnes, Sasaki & Wands 2006). Since equation (9) represents single-source local non-Gaussianity (all of the higher order terms are fully correlated with the linear term), this implies the single-source consistency relation $\tau_{\rm NL} = (6f_{\rm NL}/5)^2$. The factor of 25/9 in equation (11) is due to the conventional definition of $\tau_{\rm NL}$ in terms of the curvature perturbation ζ, related by $\zeta = 5\Phi/3$. In more general models with multiple fields contributing to Φ, the equality between the two non-linearity parameters is replaced by the SY-inequality $\tau_{\rm NL} \geq (6f_{\rm NL}/5)^2$.

4 WEAK GRAVITATIONAL LENSING

4.1 Weak lensing potential and convergence

Weak gravitational lensing probes the tidal gravitational fields of the cosmic large-scale structure by the distortion of light bundles (for reviews, please refer to Bartelmann & Schneider 2001; Bartelmann 2010). This distortion is measured by the correlated deformation of galaxy ellipticities. The projected lensing potential ψ, from which the distortion modes can be obtained by double differentiation,

$$\psi = 2\int \mathrm{d}\chi\ W_\psi(\chi)\Phi \tag{12}$$

is related to the gravitational potential Φ by projection with the weighting function $W_\psi(\chi)$,

$$W_\psi(\chi) = \frac{D_+(a)}{a}\frac{G(\chi)}{\chi}. \tag{13}$$

Born-type corrections are small for both the spectrum (Krause & Hirata 2010) and the bispectrum (Dodelson & Zhang 2005) compared to the lowest order calculation. The distribution of the lensed galaxies in redshift is incorporated in the function $G(\chi)$,

$$G(\chi) = \int_\chi^{\chi_\mathrm{H}} \mathrm{d}\chi'\ p(\chi')\frac{\mathrm{d}z}{\mathrm{d}\chi'}\left(1-\frac{\chi}{\chi'}\right) \tag{14}$$

with $\mathrm{d}z/\mathrm{d}\chi' = H(\chi')/c$. It is common in the literature to use the parametrization

$$p(z)\mathrm{d}z = p_0\left(\frac{z}{z_0}\right)^2 \exp\left(-\left(\frac{z}{z_0}\right)^\beta\right)\mathrm{d}z$$

$$\text{with}\quad \frac{1}{p_0} = \frac{z_0}{\beta}\Gamma\left(\frac{3}{\beta}\right). \tag{15}$$

Because of the linearity of the observables following from equation (12), moments of the gravitational potential are mapped on to the same moments of the observable with no mixing taking place. At this point, we would like to emphasize that the non-Gaussianity in the weak lensing signal is diluted by the line-of-sight integration, which, according to the central limit theorem, adds up a large number of non-Gaussian values for the gravitational potential with the consequence that the integrated lensing potential contains weaker non-Gaussianities (Jeong et al. 2011).

4.2 Convergence polyspectra

Application of the Limber equation and repeated substitution of $\kappa = \ell^2\psi/2$ allows the derivation of the convergence spectrum $C_\kappa(\ell)$ from the spectrum $P_\Phi(k)$ of the gravitational potential,

$$C_\kappa(\ell) = \ell^4\int_0^{\chi_\mathrm{H}}\frac{\mathrm{d}\chi}{\chi^2}\ W_\psi^2(\chi)P_\Phi(k), \tag{16}$$

of the convergence bispectrum $B_\kappa(\boldsymbol{\ell}_1,\boldsymbol{\ell}_2,\boldsymbol{\ell}_3)$,

$$B_\kappa(\boldsymbol{\ell}_1,\boldsymbol{\ell}_2,\boldsymbol{\ell}_3) = (\ell_1\ell_2\ell_3)^2\int_0^{\chi_\mathrm{H}}\frac{\mathrm{d}\chi}{\chi^4}\ W_\psi^3(\chi)B_\Phi(\boldsymbol{k}_1,\boldsymbol{k}_2,\boldsymbol{k}_3) \tag{17}$$

and of the convergence trispectrum $T_\kappa(\boldsymbol{\ell}_1,\boldsymbol{\ell}_2,\boldsymbol{\ell}_3,\boldsymbol{\ell}_4)$,

$$T_\kappa(\boldsymbol{\ell}_1,\boldsymbol{\ell}_2,\boldsymbol{\ell}_3,\boldsymbol{\ell}_4) = (\ell_1\ell_2\ell_3\ell_4)^2\int_0^{\chi_\mathrm{H}}\frac{\mathrm{d}\chi}{\chi^6}\ W_\psi^4(\chi)T_\Phi(\boldsymbol{k}_1,\boldsymbol{k}_2,\boldsymbol{k}_3,\boldsymbol{k}_4). \tag{18}$$

This relation follows from the expansion of the tensor $\psi = \partial^2\psi/\partial\theta_i\partial\theta_j$ into the basis of all symmetric 2×2 matrices provided by the Pauli matrices σ_α (Abramowitz & Stegun 1972). In particular, the lensing convergence is given by $\kappa = \mathrm{tr}(\psi\sigma_0)/2 = \Delta\psi/2$ with the unit matrix σ_0. Although the actual observable in lensing are the weak shear components $\gamma_+ = \mathrm{tr}(\psi\sigma_1)/2$ and $\gamma_\times = \mathrm{tr}(\psi\sigma_3)/2$, we present all calculations in terms of the convergence, which has identical statistical properties and being scalar, is easier to work with.

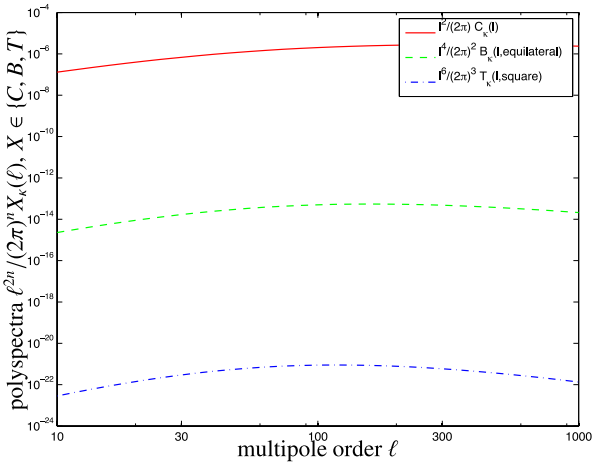

Figure 1. The weak convergence spectrum $C_\kappa(\ell)$ (red solid line), the weak convergence bispectrum for the equilateral configuration $B_\kappa(\ell)$ for an equilateral configuration (green solid line) with $f_\mathrm{NL} = 1$ and the convergence trispectrum $T_\kappa(\ell)$ for a square configuration as a function of multipole order ℓ, for $g_\mathrm{NL} = 1$ (blue dashed line).

Fig. 1 shows the weak lensing spectrum and the non-Gaussian bi- and trispectra as a function of multipole order ℓ. For the bispectrum, we choose an equilateral configuration and for the trispectrum a square one, which are in fact lower bounds on the bi- and trispectrum amplitudes for local non-Gaussianities. The polyspectra are multiplied with factors of $(\ell)^{2n}$ for making them dimensionless and in that way we were able to show all spectra in a single plot, providing a better physical interpretation of variance, skewness and kurtosis per logarithmic ℓ-interval. In our derivation, we derive the lensing potential directly from the gravitational potential, in which the polyspectra are expressed and subsequently apply ℓ^2-pre-factors to obtain the polyspectra in terms of the weak lensing convergence, for which the covariance and the noise of the measurement is most conveniently expressed. The disadvantage of this method is that the τ_NL-part of the trispectrum T_ψ diverges for the square configuration, because opposite sides of the square cancel in the $|\boldsymbol{k}_i - \boldsymbol{k}_{i+2}|$ terms which cannot be exponentiated with a negative number $n_\mathrm{s} - 4$. We control this by never letting the cosine of the angle between $\boldsymbol{k}_i$ and $\boldsymbol{k}_{i+2}$ drop below -0.95. We verified that this exclusion cone of size $\simeq 20^\circ$ has a minor influence on the computation of signal-to-noise ratios.

The contributions to the weak lensing polyspectra as a function of comoving distance χ are shown in Fig. 2, which is the derivative of Fig. 1 at fixed ℓ. At the same time, the plot presents the integrand of the Limber equation and it demonstrates nicely that the largest contribution to the weak lensing polyspectra comes from the peak of the galaxy distribution, with small variations with multipole order as higher multipoles acquire contributions from slightly lower distances.

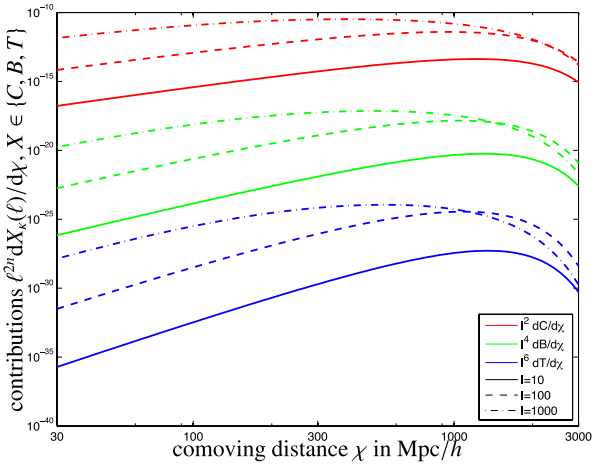

Figure 2. Contributions $dC_\kappa(\ell)/d\chi$ (red lines), $dB_\kappa(\ell)/d\chi$ (green lines) for the equilateral configuration and $dT_\kappa(\ell)/d\chi$ (blue lines) for the square configuration, as a function of comoving distance χ. The non-Gaussianity parameters are chosen to be $f_{\rm NL} = 1$ and $g_{\rm NL} = 1$. We compare the contributions at $\ell = 10$ (solid line) with $\ell = 100$ (dashed line) and $\ell = 1000$ (dash–dotted line).

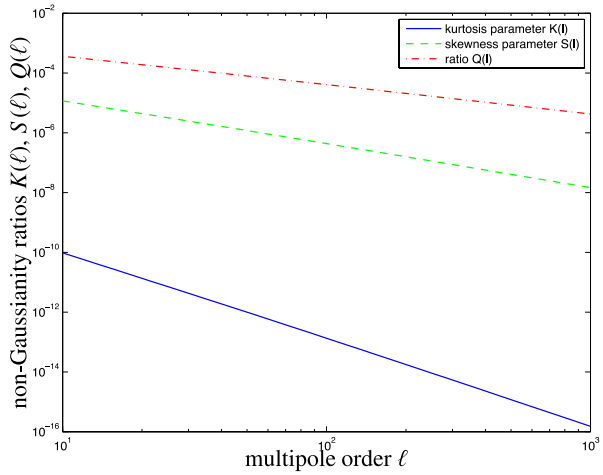

Figure 3. Parameters $K(\ell)$ (blue solid line), $S(\ell)$ (green dashed line) and $Q(\ell)$ (red dash–dotted line), where we chose an equilateral configuration for the convergence bispectrum and a square configuration for the trispectrum. The non-Gaussianity parameters are $f_{\rm NL} = 1$ and $g_{\rm NL} = 1$

4.3 Relative magnitudes of weak lensing polyspectra

The strength of the non-Gaussianity introduced by non-zero values of $g_{\rm NL}$ and $\tau_{\rm NL}$ can be quantified by taking ratios of the three polyspectra. We define the skewness parameter $S(\ell)$ as the ratio

$$S(\ell) = \frac{B_\kappa(\ell)}{C_\kappa(\ell)^{3/2}} \tag{19}$$

between the convergence bispectra for the equilateral configuration and the convergence spectrum. In analogy, we define the kurtosis parameter $K(\ell)$,

$$K(\ell) = \frac{T_\kappa(\ell)}{C_\kappa(\ell)^2}, \tag{20}$$

as the ratio between the convergence trispectrum for the square configuration and the spectrum as a way of quantifying the size of the non-Gaussianity. The relative magnitude of the bi- and trispectrum is given by the function $Q(\ell)$,

$$Q(\ell) = \frac{T_\kappa(\ell)}{B_\kappa(\ell)^{4/3}}. \tag{21}$$

For computing the three parameters, we set the non-Gaussianity parameters to $f_{\rm NL} = g_{\rm NL} = 1$.

The parameters are shown in Fig. 3 as a function of multipole order ℓ. They have been constructed such that the transfer function $T(k)$ in each of the polyspectra is cancelled. The parameters are power laws because the inflationary part of the spectrum k^{n_s-4} is scale-free and the Wick theorem reduces the polyspectra to products of that inflationary spectrum. The amplitude of the parameters reflects the proportionality of the polyspectra to $3\Omega_{\rm m}/(2\chi_{\rm H}^2)$ and the normalization of each mode proportional to σ_8. A noticeable outcome in the plot is the fact that the ratio is largest on large scales as anticipated, because the fluctuations in the inflationary fields give rise to fluctuations in the gravitational potential on which the perturbation theory is built. Since the effect of the potential is on large scale and the trispectrum is proportional to the spectrum taken to the third power, the ratio $K(\ell)$ should be the largest on large scales. Therefore, as one can see in the Fig. 3, the ratio drops to very small numbers on small scales. Similar arguments apply to $Q(\ell)$ and $S(\ell)$, although the dependences are weaker.

5 SIGNAL-TO-NOISE RATIOS

The signal strength at which a given polyspectrum can be measured is computed as the ratio between that particular polyspectrum and the variance of its estimator averaged over a Gaussian ensemble (which, in the case of structure formation non-Gaussianities, has been shown to be a serious limitation; Takada & Jain 2009; Kayo, Takada & Jain 2013; Sato & Nishimichi 2013). We work in the flat-sky approximation because the treatment of the bi- and trispectra involves a configuration space average, which requires the evaluation of Wigner symbols in multipole space.

In the flat-sky approximation, the signal-to-noise ratio $\Sigma_{\rm C}$ of the weak convergence spectrum $C_\kappa(\ell)$ reads (Tegmark, Taylor & Heavens 1997; Cooray & Hu 2001)

$$\Sigma_{\rm C}^2 = \int \frac{{\rm d}^2\ell}{(2\pi)^2} \frac{C_\kappa(\ell)^2}{{\rm cov}_{\rm C}(\ell)}, \tag{22}$$

with the Gaussian expression for the covariance ${\rm cov}_{\rm C}(\ell)$ (Hu & White 2001; Takada & Hu 2013),

$${\rm cov}_{\rm C}(\ell) = \frac{2}{f_{\rm sky}} \frac{1}{2\pi} \tilde{C}_\kappa(\ell)^2. \tag{23}$$

Likewise, the signal-to-noise ratio $\Sigma_{\rm B}$ of the bispectrum $B_\kappa(\ell)$ is given by (Hu 2000; Takada & Jain 2004; Babich 2005; Joachimi, Shi & Schneider 2009)

$$\Sigma_{\rm B}^2 = \int \frac{{\rm d}^2\ell_1}{(2\pi)^2} \int \frac{{\rm d}^2\ell_2}{(2\pi)^2} \int \frac{{\rm d}^2\ell_3}{(2\pi)^2} \frac{B_\kappa^2(\boldsymbol{\ell}_1, \boldsymbol{\ell}_2, \boldsymbol{\ell}_3)}{{\rm cov}_{\rm B}(\ell_1, \ell_2, \ell_3)}, \tag{24}$$

where the covariance ${\rm cov}_{\rm B}(\ell_1, \ell_2, \ell_3)$ follows from

$${\rm cov}_{\rm B}(\ell_1, \ell_2, \ell_3) = \frac{6\pi}{f_{\rm sky}} \frac{1}{(2\pi)^3} \tilde{C}_\kappa(\ell_1)\tilde{C}_\kappa(\ell_2)\tilde{C}_\kappa(\ell_2). \tag{25}$$

Finally, the signal-to-noise ratio $\Sigma_{\rm T}$ of the convergence trispectrum T_κ results from (Zaldarriaga 2000; Hu 2001; Kamionkowski, Smith

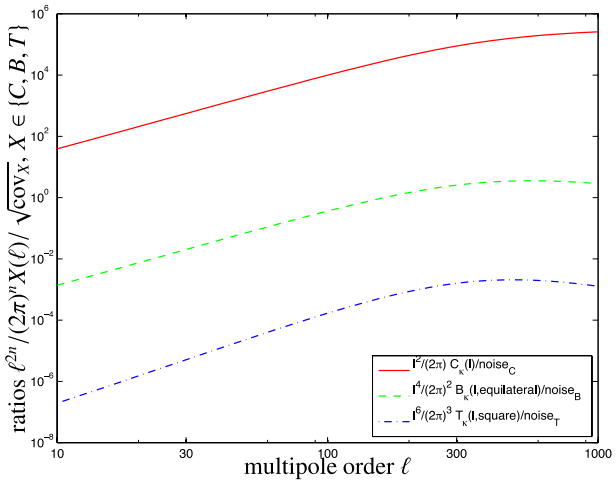

Figure 4. Noise-weighted weak lensing polyspectra: $C_\kappa(\ell)/\sqrt{\mathrm{cov}_C}$ (red solid line), $B_\kappa(\ell)/\sqrt{\mathrm{cov}_B}$ for the equilateral configuration (green dashed line) and $T_\kappa(\ell)/\sqrt{\mathrm{cov}_T}$ (blue dash–dotted line) for the square configuration. The non-Gaussianity parameters are $f_{\rm NL} = 1$ and $g_{\rm NL} = 1$.

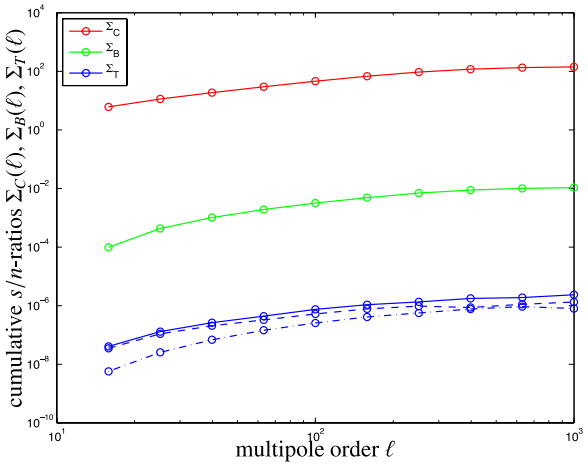

Figure 5. Cumulative signal-to-noise ratios $\Sigma_{\rm C}$ for the weak lensing spectrum (red solid line), $\Sigma_{\rm B}$ for the weak lensing bispectrum (green solid line) and $\Sigma_{\rm T}$ for the weak lensing trispectrum, for $(\tau_{\rm NL}, g_{\rm NL}) = (1, 1)$ (blue solid line), $(\tau_{\rm NL}, g_{\rm NL}) = (1, 0)$ (blue dashed line) and $(\tau_{\rm NL}, g_{\rm NL}) = (0, 1)$ (blue dash–dotted line).

& Heavens 2011)

$$\Sigma_{\rm T}^2 = \int \frac{{\rm d}^2\ell_1}{(2\pi)^2} \int \frac{{\rm d}^2\ell_2}{(2\pi)^2} \int \frac{{\rm d}^2\ell_3}{(2\pi)^2} \int \frac{{\rm d}^2\ell_4}{(2\pi)^2} \frac{T_\kappa^2(\boldsymbol{\ell}_1, \boldsymbol{\ell}_2, \boldsymbol{\ell}_3, \boldsymbol{\ell}_4)}{\mathrm{cov}_{\rm T}(\ell_1, \ell_2, \ell_3, \ell_4)}, \tag{26}$$

with the expression

$$\mathrm{cov}_{\rm T}(\ell_1, \ell_2, \ell_3, \ell_4) = \frac{24\pi}{f_{\rm sky}} \frac{1}{(2\pi)^4} \tilde{C}_\kappa(\ell_1)\tilde{C}_\kappa(\ell_2)\tilde{C}_\kappa(\ell_3)\tilde{C}_\kappa(\ell_4) \tag{27}$$

for the trispectrum covariance $\mathrm{cov}_{\rm T}(\ell_1, \ell_2, \ell_3, \ell_4)$. In all covariances, the fluctuations of the weak lensing signal and the noise are taken to be Gaussian and are therefore described by the noisy convergence spectrum $\tilde{C}_\kappa(\ell)$,

$$\tilde{C}_\kappa(\ell) = C_\kappa(\ell) + \frac{\sigma_\epsilon^2}{\bar{n}}, \tag{28}$$

with the number of galaxies per steradian $\bar{n}$ and the ellipticity noise σ_ϵ.

The configuration space integrations for estimating the signal-to-noise ratios as well as for computing Fisher matrices are carried out in polar coordinates with a Monte Carlo integration scheme (specifically, with the CUBA library by Hahn 2005, who provides a range of adaptive Monte Carlo integration algorithms). We obtained the best results with the SUAVE algorithm that uses importance sampling for estimating the values of the integrals.

Fig. 4 provides a plot of the polyspectra in units of the noise of their respective estimators. Clearly, the measurements are dominated by cosmic variance and show the according Poissonian dependence with multipole ℓ, before the galaxy shape noise limits the measurement on small scales and the curves level off or, in the case of the higher polyspectra, begin to drop on multipoles $\ell \gtrsim 300$.

An observation of the polyspectra $C_\kappa(\ell)$, B_κ and T_κ with *Euclid* would yield signal-to-noise ratios as depicted in Fig. 5. Whereas the convergence spectrum $C_\kappa(\ell)$ can be detected with high significance in integrating over the multipole range up to $\ell = 10^3$, the bispectrum would require $f_{\rm NL}$ to be of the order of 10^2 and the two trispectrum non-Gaussianities $g_{\rm NL}$ and $\tau_{\rm NL}$-values of the order of 10^6 for yielding a detection, which of course is weaker compared to CMB bounds or bounds on the parameters from large-scale structure

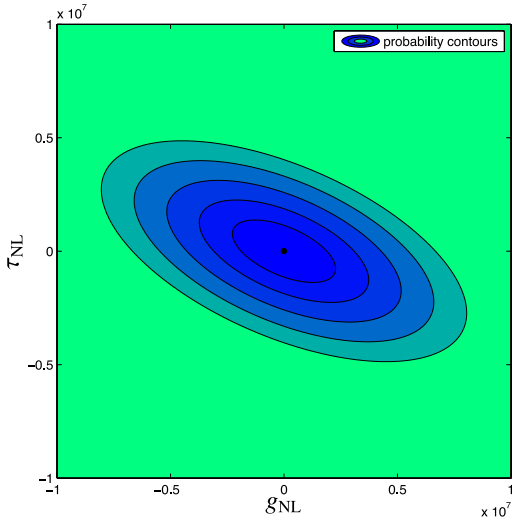

Figure 6. Degeneracies in the $g_{\rm NL}$–$\tau_{\rm NL}$-plane for a measurement with *Euclid*: the $1\sigma \ldots 4\sigma$ contours of the joint likelihood are drawn, while all cosmological parameters are assumed to be known exactly.

observation. The reason lies in the non-Gaussianity suppression due to the central-limit theorem in the line-of-sight integration (Jeong et al. 2011). This could in principle be compensated by resorting to tomographic weak lensing (see Section 10).

6 DEGENERACIES IN THE TRISPECTRUM

The independence of estimates of $g_{\rm NL}$ and $\tau_{\rm NL}$ from the weak lensing trispectrum are depicted in Fig. 6 where we plot the likelihood contours in the $g_{\rm NL}$–$\tau_{\rm NL}$-plane. The likelihood $\mathcal{L}(f_{\rm NL}, g_{\rm NL}, \tau_{\rm NL})$ is taken to be Gaussian,

$$\mathcal{L}(f_{\rm NL}, g_{\rm NL}, \tau_{\rm NL}) = \sqrt{\frac{\det(F)}{(2\pi)^3}} \exp\left[-\frac{1}{2}\begin{pmatrix} f_{\rm NL} \\ g_{\rm NL} \\ \tau_{\rm NL} \end{pmatrix}^t F \begin{pmatrix} f_{\rm NL} \\ g_{\rm NL} \\ \tau_{\rm NL} \end{pmatrix}\right], \tag{29}$$

which can be expected due to the linearity of the polyspectra with the non-Gaussianity parameters. The Fisher matrix F has been estimated for a purely Gaussian reference model and with a Gaussian covariance, and its entries can be computed in analogy to the signal-to-noise ratios. The diagonal of the Fisher matrix is composed from the values Σ_B and Σ_T with the non-Gaussianity parameters set to unity, and the only off-diagonal elements are the two entries $F_{g_{NL}\tau_{NL}}$,

$$F_{g_{NL}\tau_{NL}} = \int \frac{d^2\ell_1}{(2\pi)^2} \int \frac{d^2\ell_2}{(2\pi)^2} \int \frac{d^2\ell_3}{(2\pi)^2} \times \int \frac{d^2\ell_4}{(2\pi)^2} \frac{1}{\mathrm{cov}_T(\ell_1, \ell_2, \ell_3, \ell_4)} \times T_\kappa(g_{NL} = 1, \tau_{NL} = 0) T_\kappa(g_{NL} = 0, \tau_{NL} = 1), \quad (30)$$

which again is solved by Monte Carlo integration in polar coordinates. Essentially, the diagonal elements of the Fisher matrix are given by the inverse squared signal-to-noise ratios since $B_\kappa \propto f_{NL}$ and $T_\kappa \propto \tau_{NL}$. For Gaussian covariances, the statistical errors on f_{NL} on one side and g_{NL} and τ_{NL} on the other are independent, since $F_{f_{NL}\tau_{NL}} = 0 = F_{f_{NL}g_{NL}}$. Clearly, there is a degeneracy that g_{NL} can be increased at the expense of τ_{NL} and vice versa. In the remainder of the paper, we carry out a marginalization of the Fisher matrix such that the uncertainty in g_{NL} is contained in τ_{NL}. The overall precision that can be reached with lensing is about an order of magnitude worse compared to the CMB (Smidt et al. 2010b), with a very similar orientation of the degeneracy.

We compute the Fisher matrix on the non-Gaussianity parameters with all other cosmological parameter assumed to a level of accuracy much better than that of f_{NL}, g_{NL} and τ_{NL}, which is reasonable given the high precision one can reach with in particular tomographic weak lensing spectra, baryon acoustic oscillations and the CMB. Typical uncertainties are at least two orders of magnitude better than the constraints on non-Gaussianity from weak lensing.

7 TESTING THE SY-INEQUALITY

Given the fact that there is a vast array of different inflationary models generating local-type non-Gaussianity, it is indispensable to have a classification of these different models into some categories. This can be for instance achieved by using consistency relations among the non-Gaussianity parameters as the SY-relation. In the literature, one distinguishes between three main categories of models, the single-source model, the multisource model and constrained multisource model. As the name already reveals, the single-source model is a model of one field causing the non-linearities. The important representatives of this category include the pure curvaton and the pure modulated reheating scenarios. It is also possible that multiple sources are simultaneously responsible for the origin of density fluctuations. It could be for instance that both the inflaton and the curvaton fields are generating the non-linearities we observe today. In the case of multisource models, the relations between the non-linearity parameters are different from those for the single-source models. Finally, the constrained multisource models are models in which the loop contributions in the expressions for the power spectrum and non-linearity parameters are not neglected. The classification into these three categories was based on the relation between f_{NL} and τ_{NL} (Suyama et al. 2010). Nevertheless, this will not be enough to discriminate between the models of each category. For this purpose, we will need further relations between f_{NL} and g_{NL}. Hereby, the models are distinguished by rather if g_{NL}

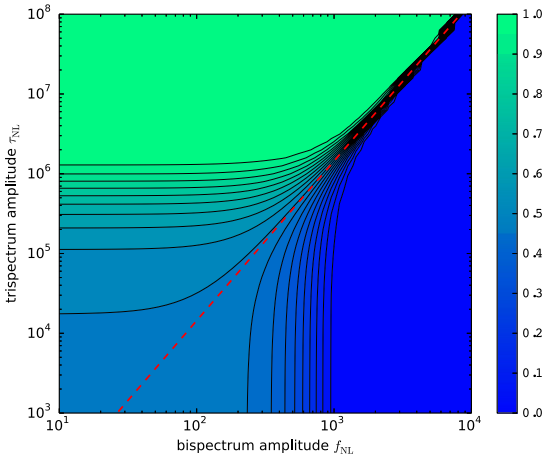

Figure 7. Bayesian evidence $\alpha(f_{NL}, \tau_{NL})$ in the f_{NL}–τ_{NL}-plane. Blue regions correspond to low, green regions to high degrees of belief. The SY-relation $\tau_{NL} = (6f_{NL}/6)^2$ is indicated by the red dashed line.

is proportional to f_{NL} ($f_{NL} \sim g_{NL}$) or enhanced or suppressed compared to f_{NL}. Summarizing, the f_{NL}–τ_{NL} and f_{NL}–g_{NL} relations will be powerful tools to discriminate models well. In this work, we are focusing on the SY-relation between f_{NL} and τ_{NL}. The Bayesian evidence (for reviews, see Trotta 2007, 2008) for the SY-relation $\tau_{NL} \geq (6f_{NL}/5)^2$ can be expressed as the fraction α of the likelihood $\mathcal{L}$ that provides support:

$$\alpha = \int_{\tau_{NL} \geq (6f_{NL}/5)^2} d\tau'_{NL} \int df'_{NL}\, \mathcal{L}\left(f_{NL} - f'_{NL}, \tau_{NL} - \tau'_{NL}\right). \quad (31)$$

Hence, α answers the question as to how likely one would believe in the SY-inequality with inferred f'_{NL} and τ'_{NL}-values if the true values are given by f_{NL} and τ_{NL}. Technically, α corresponds to the integral over the likelihood in the f_{NL}–τ_{NL}-plane over the allowed region. If $\alpha = 1$, we would fully believe in the SY-inequality, if $\alpha = 0$ we would think that the SY-relation is violated. Correspondingly, $1 - \alpha$ would provide a quantification of the violation of the SY-relation,

$$1 - \alpha = \int_{\tau_{NL} < (6f_{NL}/5)^2} d\tau'_{NL} \int df'_{NL}\, \mathcal{L}\left(f_{NL} - f'_{NL}, \tau_{NL} - \tau'_{NL}\right). \quad (32)$$

We can formulate the integration over the allowed region as well as an integration over the full f_{NL}–τ_{NL}-range of the likelihood multiplied with the Heaviside function,

$$\alpha = \int d\tau'_{NL} \int df'_{NL} \mathcal{L}(f_{NL} - f'_{NL}, \tau_{NL} - \tau'_{NL}) \Theta(\tau_{NL} - (6/5 f_{NL})^2). \quad (33)$$

This function would play the role of a theoretical prior in the f_{NL}–τ_{NL}-plane. In this interpretation, α corresponds to the Bayesian evidence, that means the degree of belief that the SY-inequality is correct.

We can test the SY-inequality $\tau_{NL} \geq (6f_{NL}/5)^2$ up to the errors on f_{NL} and τ_{NL} provided by the lensing measurement. Fig. 7 shows the test statistic $\alpha(f_{NL}, g_{NL}, \tau_{NL})$ in the f_{NL}–τ_{NL}-plane, where the likelihood has been marginalized over the parameter g_{NL}. The blue regime $f_{NL} \gtrsim 10^2$ is the parameter space which would not fulfill the SY-inequality, whereas the green area $\tau_{NL} \gtrsim 10^5$ is the parameter space where the SY-relation would be fulfilled. Values of

$f_{\rm NL} \lesssim 10^2$ and $\tau_{\rm NL} \lesssim 10^5$ are inconclusive and even though non-Gaussianity parameters may be inferred that would be in violation of the SY-relation, the wide likelihood would not allow us to derive a statement. Another nice feature is the fact that for large $f_{\rm NL}$ and $\tau_{\rm NL}$, the relation can be probed to larger precision and the contours are more closely spaced.

In models where the field which generates non-Gaussianity has a quadratic potential, the non-Gaussianity is mainly captured by $f_{\rm NL}$, while $g_{\rm NL}$ is negligible. An example is the curvaton scenario, it is only through self-interactions of the curvaton that $g_{\rm NL}$ may become large (Enqvist et al. 2010).

8 ANALYTICAL DISTRIBUTIONS

In this section, we derive the analytical expression for the probability density that the SY-relation is exactly fulfilled, $\tau_{\rm NL} = (6f_{\rm NL}/5)^2$, i.e. for the case $(6f_{\rm NL}/5)^2/\tau_{\rm NL} \equiv 1$. For this purpose, we explore the properties of the distribution

$$p(Q)\mathrm{d}Q \quad \text{with} \quad Q = \frac{(6f_{\rm NL}/5)^2}{\tau_{\rm NL}}, \tag{34}$$

where the parameters $f_{\rm NL}$ and $\tau_{\rm NL}$ are both Gaussian distributed with means $\bar{f_{\rm NL}}$, $\bar{\tau_{\rm NL}}$ and widths $\sigma_{f_{\rm NL}}$ and $\sigma_{\tau_{\rm NL}}$.

We will split the derivation into two parts. First of all, we will derive the distribution for the product $f_{\rm NL}^2$. For this purpose, we use the transformation of the probability density:

$$p_y(y)\mathrm{d}y = p_x(x)\mathrm{d}x \tag{35}$$

with the Jacobian $\mathrm{d}x/\mathrm{d}y = 1/(2\sqrt{y})$ and where $x = f_{\rm NL}$ and $y = x^2$. Thus, we can write the above equality as

$$p_y(y) = \frac{p_x(\sqrt{y})}{2\sqrt{y}}, \tag{36}$$

where the probability distribution $p_x(x)$ is given by

$$p_x(\sqrt{y}) = \frac{1}{\sqrt{2\pi\sigma^2_{f_{\rm NL}}}} \exp\left(-\frac{(\sqrt{y} - \bar{f_{\rm NL}})^2}{2\sigma^2_{f_{\rm NL}}}\right). \tag{37}$$

Naively written in this way, we would lose half of the distribution and do not obtain the right normalization. Therefore, we have to distinguish between the different signs of y. The distribution of a square of a Gaussian distributed variate $f_{\rm NL}$ with mean $\bar{f_{\rm NL}}$ and variance $\sigma_{f_{\rm NL}}$ is given by

$$p_y(y) = \frac{1}{\sqrt{2\pi\sigma^2_{f_{\rm NL}}}} \frac{1}{2\sqrt{y}} \times \begin{cases} \exp\left(-\frac{(\sqrt{y}-\bar{f_{\rm NL}})^2}{2\sigma^2_{f_{\rm NL}}}\right), & \text{positive branch of } \sqrt{y} \\ \exp\left(-\frac{(-\sqrt{y}-\bar{f_{\rm NL}})^2}{2\sigma^2_{f_{\rm NL}}}\right), & \text{negative branch of } \sqrt{y} \end{cases} \tag{38}$$

with $y = f_{\rm NL}^2$. In the special case of normally distributed variates, the above expression would reduce to

$$p_y(y) = \frac{1}{\pi\sigma_{f_{\rm NL}}\sigma_{\tau_{\rm NL}}} K_0\left(\frac{|y|}{\sigma_{f_{\rm NL}}\sigma_{\tau_{\rm NL}}}\right), \tag{39}$$

where $K_n(y)$ is a modified Bessel function of the second kind (Abramowitz & Stegun 1972).

The next step is now to implement the distribution equation (38) into a ratio distribution since we are interested in the distribution of $(6f_{\rm NL}/5)^2/\tau_{\rm NL}$ incorporating the additional factor. The ratio distribution can be written down using the Mellin transformation (Arfken & Weber 2005):

$$p(Q) = \int |\alpha| \mathrm{d}\alpha \; p_y(\alpha Q, \bar{f_{\rm NL}}) p_z(\alpha, \bar{\tau_{\rm NL}}), \tag{40}$$

with a Gaussian distribution for $z = \tau_{\rm NL}$,

$$p_z(z) = \frac{1}{\sqrt{2\pi\sigma_z^2}} \exp\left(-\frac{(z-\bar{z})^2}{2\sigma_z^2}\right). \tag{41}$$

In the special case of Gaussian distributed variates with zero mean, the distribution would be simply given by the Cauchy distribution (Marsaglia 1965, 2006), but in the general case, equation (38) needs to be evaluated analytically.

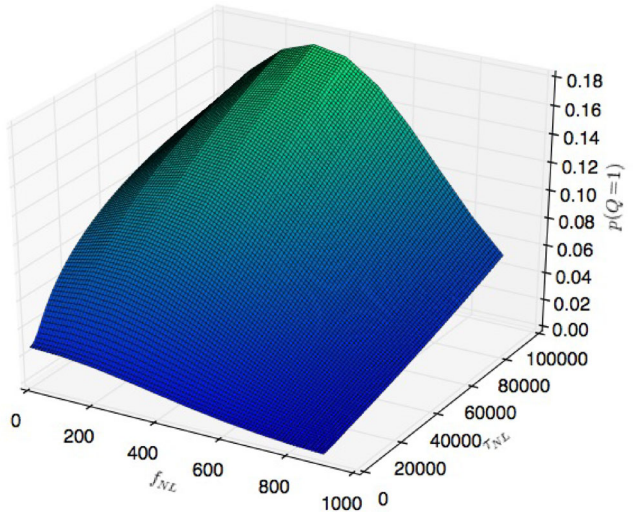

Figure 8. The probability distribution $p(Q)\mathrm{d}Q$ of $Q = (6f_{\rm NL}/5)^2/\tau_{\rm NL}$ as a function of the non-Gaussianity parameters $f_{\rm NL}$ and $\tau_{\rm NL}$.

In Fig. 8, we are illustrating the ratio distribution as a function of $f_{\rm NL}$ and $\tau_{\rm NL}$ for $Q = 1$, i.e. for the case where the SY-relation becomes an equality. The values for $f_{\rm NL}$ run from 1 to 10^3 and $\tau_{\rm NL}$ runs from 1 to 10^6. The variances $\sigma_{f_{\rm NL}}$ and $\sigma_{\tau_{\rm NL}}$ are taken from the output of the Fisher matrix and correspond to $\sigma_{f_{\rm NL}} = 93$ and $\sigma_{\tau_{\rm NL}} = 7.5 \times 10^5$. We would like to point out the nice outcome, that the distribution has a clearly visible bumped line along the SY-equality. Similarly, Fig. 9 shows a number of example distributions $p(Q)\mathrm{d}Q$ for a choice of non-Gaussianity parameters $f_{\rm NL}$ and $\tau_{\rm NL}$. We let Q run from 1 to 5 and fix the values $f_{\rm NL} = 10^2, 10^3$ and $\tau_{\rm NL} = 10^4, 10^5, 10^6$.

Smidt et al. (2010b) study possible bounds on $A_{\rm NL} = 1/Q$ based on a combination of CMB probes. The value of $f_{\rm NL} = 32$ suggested by *WMAP*7 (Komatsu et al. 2011) would imply that a a detection of $\tau_{\rm NL}$ with *Planck* is possible if $Q < 1/2$, and future experiments such as COrE (The COrE Collaboration: Armitage-Caplan et al. 2011) or EPIC (Bock et al. 2008) can probe regions of smaller trispectra, which might be relevant as a number of models predict small bi- and large trispectra, and could be a favourable for detecting non-Gaussianities. In our work, we prefer to work with the probability distribution of Q because for small values of $f_{\rm NL}$ as suggested by Planck (Planck Collaboration: Ade et al. 2013a) one naturally obtains large values for $A = 1/Q$.

9 BAYESIAN EVIDENCE FOR A VIOLATION OF THE SY-EQUALITY

An interesting quantity from a Bayesian point of view is the evidence ratio provided by a measurement comparing a model in which the

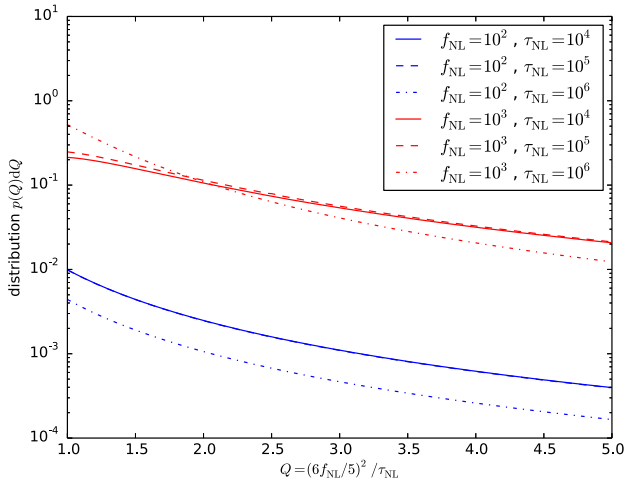

Figure 9. The probability distribution $p(Q)$ as a function of Q for fixed non-Gaussianity parameter $f_{\rm NL} = 10^2, 10^3$ (red and blue, respectively), and $\tau_{\rm NL} = 10^4, 10^5, 10^6$ (solid, dashed and dash–dotted).

SY-equality is fulfilled ($\tau_{\rm NL} = (6f_{\rm NL}/5)^2$) in contrast to the model with an SY-violation ($\tau_{\rm NL} \geq (6f_{\rm NL}/5)^2$). Following Trotta (2007, 2008), we define the pieces of evidence E for either model,

$$E_{=} = \int \mathrm{d}f'_{\rm NL}\; p_{=}(f'_{\rm NL}) p_{\rm CMB}(f'_{\rm NL}) \tag{42}$$

$$E_{\geq} = \int \mathrm{d}f'_{\rm NL}\; p_{\geq}(f'_{\rm NL}) p_{\rm CMB}(f'_{\rm NL}) \tag{43}$$

with a prior on the two non-Gaussianity parameters from the CMB, whose functional shape we assume to be Gaussian. The two distributions $p_{=}(f_{\rm NL})\mathrm{d}f_{\rm NL}$ and $p_{\geq}(f_{\rm NL})\mathrm{d}f_{\rm NL}$ originate from a joint Gaussian on $f_{\rm NL}$ and $\tau_{\rm NL}$ with the Fisher matrix as the inverse covariance where the conditions $\tau_{\rm NL} = (6f_{\rm NL}/5)^2$ and $\tau_{\rm NL} \geq (6f_{\rm NL}/5)^2$ are integrated out,

$$p_{=}(f'_{\rm NL}) = \int \mathrm{d}\tau'_{\rm NL} \mathcal{L}(f_{\rm NL} - f'_{\rm NL}, \tau_{\rm NL} - \tau'_{\rm NL}) \delta_D \left(\tau_{\rm NL} - (6/5 f_{\rm NL})^2\right) \tag{44}$$

$$p_{\geq}(f'_{\rm NL}) = \int \mathrm{d}\tau'_{\rm NL} \mathcal{L}(f_{\rm NL} - f'_{\rm NL}, \tau_{\rm NL} - \tau'_{\rm NL}) \Theta \left(\tau_{\rm NL} - (6/5 f_{\rm NL})^2\right) \tag{45}$$

such that $E_{\geq}$ is equal to α up to the prior. Effectively, the SY-relation is used as a marginalization condition. Finally, the Bayes ratio $B = E_{=}/E_{\geq}$ can be used to decide between the two models given the measurement and the prior, as it quantifies the model complexity needed for explaining the data. As a CMB prior on $f_{\rm NL}$, we assume a Gaussian with width $\sigma_{f_{\rm NL}} \simeq 10$. Fig. 10 suggests the preference of $E_{=}$ over $E_{\geq}$ over almost the entire parameter range, with the exception of $\tau_{\rm NL} \gg f_{\rm NL}$ in the upper-left corner.

10 SUMMARY

The topic of this paper is an investigation of inflationary bi- and trispectra by weak lensing, and testing of the SY-inequality relating the relative strengths of the inflationary bi- and trispectrum amplitudes using weak lensing as a mapping of the large-scale structure. Specifically, we consider the case of the projected *Euclid* weak lensing survey and choose a basic wCDM cosmology as the background model.

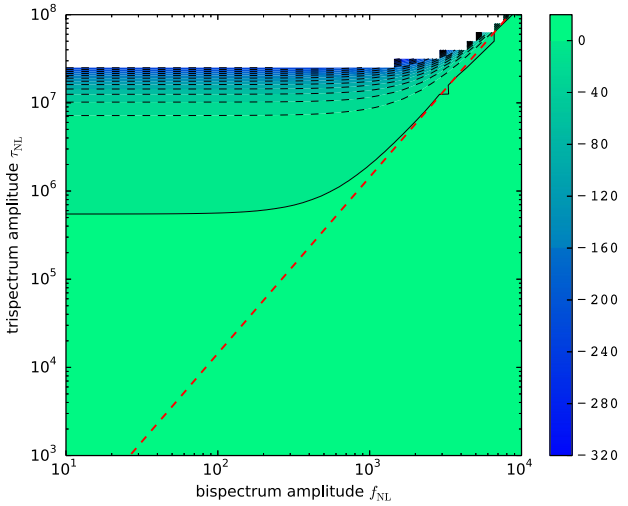

Figure 10. Logarithm of the Bayesian evidence ratio $E_{=}/E_{\geq}$, indicating that for most of the parameter range preference is given to the simpler hypothesis $E_{=}$, only in the parameter region $\tau_{\rm NL} \gg f_{\rm NL}$ the hypothesis $E_{\geq}$ is preferred.

(i) We compute weak lensing potential and weak lensing convergence spectra C_κ, bispectra B_κ and trispectra T_κ by Limber projection from the CDM polyspectra P_Φ, B_Φ and T_Φ of the Newtonian gravitational potential Φ. The non-Gaussianity model for the higher order spectra are local non-Gaussianities parametrized with $f_{\rm NL}$, $g_{\rm NL}$ and $\tau_{\rm NL}$. The weak lensing polyspectra reflect in their magnitude the perturbative ansatz by which they are generated and collect most of their amplitude at distances of $\sim$1 Gpc h^{-1}, where the higher order polyspectra show a tendency to be generated at slightly smaller distances. Ratios of polyspectra where the transfer function has been divided out, nicely illustrate the reduction to products of spectra by application of the Wick theorem, as a pure power-law behaviour is recovered by this construction.

(ii) The signal-to-noise ratios $\Sigma_{\rm C}$, $\Sigma_{\rm B}$ and $\Sigma_{\rm T}$ at which the polyspectra can be estimated with *Euclid*'s weak lensing data are forecasted using a very efficient Monte Carlo integration scheme for carrying out the configuration space summation. These integrations are carried out in flat polar coordinates with a Gaussian expression for the signal covariance. Whereas the first simplification should influence the result only weakly as most of the signal originates from sufficiently large multipoles, the second simplification has been shown to be violated in the investigation of dominating structure formation non-Gaussianities, but might be applicable in the case of weak inflationary non-Gaussianities and on low multipoles.

(iii) With a very similar integration scheme, we compute a Fisher matrix for the set of non-Gaussianity parameters $f_{\rm NL}$, $g_{\rm NL}$ and $\tau_{\rm NL}$ such that a Gaussian likelihood $\mathcal{L}$ can be written down. Marginalization over $g_{\rm NL}$ yields the final likelihood $\mathcal{L}(f_{\rm NL}, \tau_{\rm NL})$ which is the basis of the statistical investigations concerning the SY-inequality. The diagonal elements of the Fisher matrix are simply inverse squared signal-to-noise ratios due to the proportionality $B_\kappa \propto f_{\rm NL}$ and $T_\kappa \propto \tau_{\rm NL}$. For Gaussian covariances, the parameters $f_{\rm NL}$ and $\tau_{\rm NL}$ are statistically independent.

(iv) We quantify the degree of belief in the SY-relation with a set of inferred values for $f_{\rm NL}$ and $\tau_{\rm NL}$ and with statistical errors $\sigma_{f_{\rm NL}}$ and $\sigma_{\tau_{\rm NL}}$ by computing the Bayesian evidence that the SY-relation $\tau_{\rm NL} \geq (6f_{\rm NL}/5)^2$ is fulfilled. *Euclid* data would provide evidence in favour of the relation for $\tau_{\rm NL} \gtrsim 10^5$ and against the relation if

$f_{\rm NL} \gtrsim 10^2$. For $f_{\rm NL} < 10^2$ and $\tau_{\rm NL} \lesssim 10^5$, the Bayesian evidence is inconclusive and quite generally, larger non-Gaussianities allow for a better probing of the relation. Comparing the Bayesian evidence of an equality in comparison to an inequality suggests that the equality is preferred as an explanation of the data given the amount of statistical error expected from the weak lensing measurement and that distinguishing between the two cases is difficult, except for extreme cases where $\tau_{\rm NL} \gg f_{\rm NL}$.

(v) We provide a computation of the probability that the quantity $Q \equiv (6f_{\rm NL}/5)^2/\tau_{\rm NL}$ is one, i.e. for an exact SY-relation. The distribution can be derived by generating a χ^2-distribution for $f_{\rm NL}^2$ and then by Mellin transform for the ratio $f_{\rm NL}^2/\tau_{\rm NL}$. We observe, that the analytical probability distribution has a clearly visible bumped line along the SY-equality.

In summary, we would like to point out that constraining non-Gaussianities in weak lensing data is possible but the sensitivity is weaker compared to other probes. Nevertheless, for the small bispectrum parameter confirmed by *Planck*, $\tau_{\rm NL}$ values of the order of 10^5 would be needed to claim a satisfied SY-relation, and values smaller than that would not imply a violation, given the large experimental uncertainties. If we assume that the non-linearity parameters are completely scale independent, then the *Planck* constraints of $-9.1 < f_{\rm NL} < 14$ and $\tau_{\rm NL} < 2800$ (both bounds are quoted at the 95 per cent confidence limit) push us towards the region on the lower left-hand side of Fig. 7, where the observational data are not able to discriminate whether the SY-inequality is saturated, holds or is broken. However, if non-Gaussianity is larger on small scales, or if the sensitivity of weak lensing data can be significantly improved using tomography then a more positive conclusion might be reached.

Despite the fact that we will not be able to see a violation of the inequality, if $\tau_{\rm NL}$ is large enough to be observed, then this together with the tight observational constraints on $f_{\rm NL}$ will imply that the single-source relation is broken and instead $\tau_{\rm NL} \gg f_{\rm NL}^2$. Even though this is allowed by inflation, such a result would come as a surprise and be of great interest, since typically even multisource scenarios predict a result which is close to the single-source equality, and a strong breaking is hard to realize for known models, e.g. Peterson & Tegmark (2011), Elliston et al. (2012), Leung et al. (2013), although examples can be constructed at the expense of fine tuning (Ichikawa et al. 2008; Byrnes, Choi & Hall 2009).

As an outlook, we provide a very coarse projection what levels of $f_{\rm NL}$ and $\tau_{\rm NL}$ can be probed by tomographic surveys (Hu 1999; Takada & Jain 2004) with $N = 2, 3, 4$ redshift bins which are chosen to contain equal fractions of the galaxy distribution, as a way of boosting the sensitivity, to decrease statistical errors and break degeneracies (Kitching, Taylor & Heavens 2008; Schäfer & Heisenberg 2012), in our case on the non-Gaussianity parameters. The binning was idealized with a fraction $1/n_{\rm bin}$ of galaxies in each of the $n_{\rm bin}$ bins, and without taking redshift errors into account. The shape noise was assumed to be $n_{\rm bin} \times \sigma_\epsilon^2/n$ with the total number n of galaxies per steradian and $\sigma\epsilon \simeq 0.3$. Fig. 11 shows the signal-to-noise ratio $\Sigma_{\rm B}$ and $\Sigma_{\rm T}$ for measuring local weak lensing bi- and trispectra, respectively, and at the same time those numbers correspond to the inverse statistical errors $\sigma_{f_{\rm NL}}$ and $\sigma_{\tau_{\rm NL}}$ because of the proportionality $B_\kappa \propto f_{\rm NL}$ and $T_\kappa \propto \tau_{\rm NL}$. Taking the full covariance between lensing bi- and trispectra into account yields an improvement on the error on $f_{\rm NL}$ by about 40 per cent and on $\tau_{\rm NL}$ by about 50 per cent. These numbers are valid for the planned *Euclid* survey. Of course, many systematical effects become important, related to the measurement itself (Semboloni et al. 2011a; Heymans et al. 2013), to structure formation non-Gaussianities at low redshifts (which can in principle be controlled with good priors on cosmological parameters; Schäfer et al. 2012), or to the numerics of the polyspectrum estimation (Smith, Kamionkowski & Wandelt 2011a).

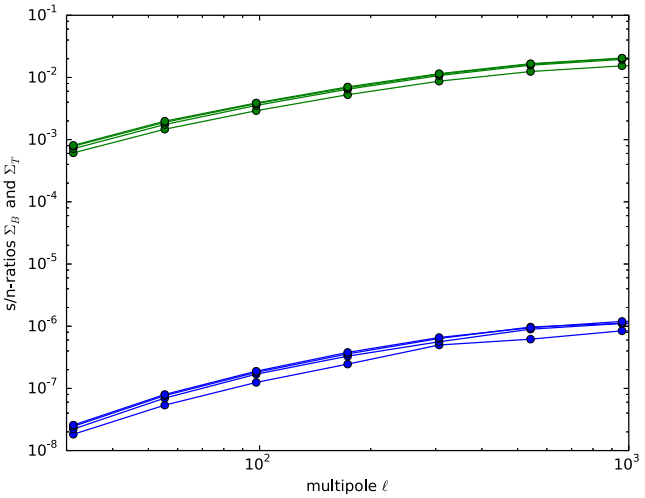

Figure 11. Cumulative signal-to-noise ratios $\Sigma_{\rm B}$ (green lines) and $\Sigma_{\rm T}$ (blue lines) for measuring the convergence bi- and trispectrum in a tomographic weak lensing survey, with $N = 1, 2, 3, 4$ (bottom to top) redshift bins.

ACKNOWLEDGEMENTS

AG's and BMS's work was supported by the German Research Foundation (DFG) within the framework of the excellence initiative through GSFP+ at Heidelberg and the International Max Planck Research School for astronomy and cosmic physics. LH was supported by the Swiss Science Foundation and CTB acknowledges support from the Royal Society. We would like to thank Gero Jürgens for his support concerning the expressions for the covariance of bi- and trispectra. LH would like to thank to Claudia de Rham and Raquel Ribeiro for very useful discussions. Finally, we would like to express our gratitude to the anonymous referee for thoughtful questions.

REFERENCES

Abramowitz M., Stegun I. A., 1972, Handbook of Mathematical Functions. Dover Press, New York
Amara A., Réfrégier A., 2007, MNRAS, 381, 1018
Arfken G. B., Weber H. J., 2005, Mathematical Methods for Physicists, 6th ed. Elsevier, Amsterdam
Assassi V., Baumann D., Green D., 2012, J. Cosmol. Astropart. Phys., 1211, 047
Babich D., 2005, Phys. Rev. D, 72, 043003
Bardeen J. M., Bond J. R., Kaiser N., Szalay A. S., 1986, ApJ, 304, 15
Bartelmann M., 2010, Class. Quantum Gravity, 27, 233001
Bartelmann M., Schneider P., 2001, Phys. Rep., 340, 291
Bartolo N., Komatsu E., Matarrese S., Riotto A., 2004, Phys. Rep., 402, 103
Becker A., Huterer D., Kadota K., 2011, J. Cosmol. Astropart. Phys., 1101, 006
Beltrán Almeida J. P., Rodríguez Y., Valenzuela-Toledo C. A., 2013, Mod. Phys. Lett. A, 28, 50012
Bennett C. L. et al., 2013, ApJS, 208, 20
Bernardeau F., van Waerbeke L., Mellier Y., 2003, A&A, 397, 405
Bock J. et al., 2008, preprint (arXiv:0805.4207)
Byrnes C. T., Sasaki M., Wands D., 2006, Phys. Rev. D, 74, 123519

Byrnes C. T., Choi K.-Y., Hall L. M., 2009, J. Cosmol. Astropart. Phys., 0902, 017
Byrnes C. T., Enqvist K., Takahashi T., 2010a, J. Cosmol. Astropart. Phys., 1009, 026
Byrnes C. T., Gerstenlauer M., Nurmi S., Tasinato G., Wands D., 2010b, J. Cosmol. Astropart. Phys., 1010, 004
Byun J., Bean R., 2013, J. Cosmol. Astropart. Phys., 1309, 026
Chen X., 2005, Phys. Rev. D, 72, 123518
Cooray A., Hu W., 2001, ApJ, 554, 56
Desjacques V., Seljak U., 2010a, Class. Quantum Gravity, 27, 124011
Desjacques V., Seljak U., 2010b, Adv. Astron., 2010, 908640
Dodelson S., Zhang P., 2005, Phys. Rev. D, 72, 083001
Elliston J., Alabidi L., Huston I., Mulryne D., Tavakol R., 2012, J. Cosmol. Astropart. Phys., 1209, 001
Enqvist K., Nurmi S., Taanila O., Takahashi T., 2010, J. Cosmol. Astropart. Phys., 1004, 009
Enqvist K., Hotchkiss S., Taanila O., 2011, J. Cosmol. Astropart. Phys., 1104, 017
Fedeli C., Pace F., Moscardini L., Grossi M., Dolag K., 2011a, MNRAS, 416, 3098
Fedeli C., Carbone C., Moscardini L., Cimatti A., 2011b, MNRAS, 414, 1545
Fergusson J. R., Shellard E. P. S., 2007, Phys. Rev. D, 76, 083523
Fergusson J., Shellard E., 2009, Phys. Rev. D, 80, 043510
Fergusson J. R., Liguori M., Shellard E. P. S., 2010a, Phys. Rev. D, 82, 023502
Fergusson J. R., Regan D. M., Shellard E. P. S., 2010b, preprint (arXiv:1012.6039)
Giannantonio T., Ross A. J., Percival W. J., Crittenden R., Bacher D. et al., 2014, Phys. Rev. D, 89, 023511
Hahn T., 2005, Comput. Phys. Commun., 168, 78
Heymans C. et al., 2013, MNRAS, 432, 2433
Hikage C., Matsubara T., 2012, MNRAS, 425, 2187
Hikage C., Matsubara T., Coles P., Liguori M., Hansen F. K., Matarrese S., 2008, MNRAS, 389, 1439
Hu W., 1999, ApJ, 522, L21
Hu W., 2000, Phys. Rev. D, 62, 043007
Hu W., 2001, Phys. Rev. D, 64, 083005
Hu W., White M., 2001, ApJ, 554, 67
Ichikawa K., Suyama T., Takahashi T., Yamaguchi M., 2008, Phys.Rev. D, 78, 063545
Jeong D., Schmidt F., Sefusatti E., 2011, Phys. Rev. D, 83, 123005
Joachimi B., Shi X., Schneider P., 2009, A&A, 508, 1193
Kamionkowski M., Smith T. L., Heavens A., 2011, Phys. Rev. D, 83, 023007
Kayo I., Takada M., Jain B., 2013, MNRAS, 429, 344
Kehagias A., Riotto A., 2012, Nucl. Phys. B, 864, 492
Kitching T. D., Taylor A. N., Heavens A. F., 2008, MNRAS, 389, 173
Komatsu E., 2010, Class. Quantum Gravity, 27, 124010
Komatsu E. et al., 2009, preprint (arXiv:0902.4759)
Komatsu E. et al., 2011, ApJS, 192, 18
Krause E., Hirata C. M., 2010, A&A, 523, A28
Lesgourgues J., 2013, preprint (arXiv:1302.4640)
Leung G., Tarrant E. R. M., Byrnes C. T., Copeland E. J., 2013, J. Cosmol. Astropart. Phys., 1308, 006
Lewis A., 2011, J. Cosmol. Astropart. Phys., 1110, 026
Linder E. V., Jenkins A., 2003, MNRAS, 346, 573
Lo Verde M., Miller A., Shandera S., Verde L., 2008, J. Cosmol. Astropart. Phys., 2004, 14
LoVerde M., Smith K. M., 2011, J. Cosmol. Astropart. Phys., 1108, 003
Marian L., Hilbert S., Smith R. E., Schneider P., Desjacques V., 2011, ApJ, 728, L13
Marsaglia G., 1965, J. Am. Stat. Assoc., 60, 193
Marsaglia G., 2006, J. Stat. Softw., 16, 1
Martin J., Ringeval C., Vennin V., 2013, preprint (arXiv:1303.3787)
Ménard B., Bartelmann M., Mellier Y., 2003, A&A, 409, 411
Munshi D., van Waerbeke L., Smidt J., Coles P., 2012, MNRAS, 419, 536
Pace F., Moscardini L., Bartelmann M., Branchini E., Dolag K., Grossi M., Matarrese S., 2011, MNRAS, 411, 595
Peterson C. M., Tegmark M., 2011, Phys. Rev. D, 84, 023520
Pettinari G. W., Fidler C., Crittenden R., Koyama K., Wands D., 2013, J. Cosmol. Astropart. Phys., 1304, 003
Planck Collaboration:, Ade P. A. R. et al., 2013a, preprint (arXiv:1303.5082)
Planck Collaboration:, Ade P. A. R. et al., 2013b, preprint (arXiv:1303.5076)
Refregier A., 2009, Exp. Astron., 23, 17
Riotto A., Sloth M. S., 2011, Phys. Rev. D, 83, 041301
Rodríguez Y., Beltrán Almeida J. P., Valenzuela-Toledo C. A., 2013, J. Cosmol. Astropart. Phys., 1304, 039
Sato M., Nishimichi T., 2013, Phys. Rev. D, 87, 123538
Schäfer B. M., Heisenberg L., 2012, MNRAS, 423, 3445
Schäfer B. M., Grassi A., Gerstenlauer M., Byrnes C. T., 2012, MNRAS, 421, 797
Seery D., Lidsey J. E., Sloth M. S., 2007, J. Cosmol. Astropart. Phys., 0701, 027
Sefusatti E., Liguori M., Yadav A. P., Jackson M. G., Pajer E., 2009, J. Cosmol. Astropart. Phys., 0912, 022
Sekiguchi T., Sugiyama N., 2013, J. Cosmol. Astropart. Phys., 1309, 002
Semboloni E., Heymans C., van Waerbeke L., Schneider P., 2008, MNRAS, 388, 991
Semboloni E., Hoekstra H., Schaye J., van Daalen M. P., McCarthy I. G., 2011a, MNRAS, 417, 2020
Semboloni E., Schrabback T., van Waerbeke L., Vafaei S., Hartlap J., Hilbert S., 2011b, MNRAS, 410, 143
Smidt J., Amblard A., Cooray A., Heavens A., Munshi D., Serra P., 2010a, preprint (arXiv:e-prints)
Smidt J., Amblard A., Byrnes C. T., Cooray A., Heavens A., Munshi D., 2010b, Phys. Rev. D, 81, 123007
Smith T. L., Kamionkowski M., Wandelt B. D., 2011a, Phys. Rev. D, 84, 063013
Smith K. M., Loverde M., Zaldarriaga M., 2011b, Phys. Rev. Lett., 107, 191301
Sugiyama N., 1995, ApJS, 100, 281
Sugiyama N. S., 2012, J. Cosmol. Astropart. Phys., 1205, 032
Sugiyama N. S., Komatsu E., Futamase T., 2011, Phys. Rev. Lett., 106, 251301
Suyama T., Yamaguchi M., 2008, Phys. Rev. D, 77, 023505
Suyama T., Takahashi T., Yamaguchi M., Yokoyama S., 2010, J. Cosmol. Astropart. Phys., 1012, 030
Takada M., Hu W., 2013, Phys. Rev. D, 87, 123504
Takada M., Jain B., 2003, MNRAS, 344, 857
Takada M., Jain B., 2004, MNRAS, 348, 897
Takada M., Jain B., 2009, MNRAS, 395, 2065
Tasinato G., Byrnes C. T., Nurmi S., Wands D., 2013, Phys. Rev. D, 87, 043512
Tegmark M., Taylor A. N., Heavens A. F., 1997, ApJ, 480, 22
The COrE Collaboration:, Armitage-Caplan C. et al., 2011, preprint (arXiv:1102.2181)
Trotta R., 2007, MNRAS, 378, 72
Trotta R., 2008, Contemp. Phys., 49, 71
Turner M. S., White M., 1997, Phys. Rev. D, 56, 4439
Verde L., 2010, Adv. Astron., 2010
Vielva P., Sanz J. L., 2009, MNRAS, 397, 837
Wang Y., 2013, preprint (arXiv:1303.1523)
Wang L., Steinhardt P. J., 1998, ApJ, 508, 483
Zaldarriaga M., 2000, Phys. Rev. D, 62, 063510

This paper has been typeset from a TEX/LATEX file prepared by the author.